PERFORMANCE OF DOPPLER ESTIMATION FOR ACOUSTIC SOURCES WITH ATMOSPHERIC SCATTERING

Richard J. Kozick

Bucknell University
Department of Electrical Engineering
Lewisburg, Pennsylvania 17837

Brian M. Sadler

Army Research Laboratory
2800 Powder Mill Road
Adelphi, Maryland 20783

ABSTRACT

A statistical analysis of differential Doppler estimation is presented for acoustic sources with a harmonic spectrum. Our model for the sensor measurements includes a physics-based statistical model for the scattering of the wavefronts by the atmosphere. We derive the Cramér-Rao bound (CRB) on differential Doppler estimation as a function of the atmospheric conditions, the frequency of the source, and the range of the source. We apply the CRB result for several cases of interest with simulated and measured data.

1. INTRODUCTION

The data collected by a network of aeroacoustic sensors may be processed to localize the positions of ground vehicles, track the vehicles as they move, and identify the type of vehicle. However, this processing is challenging because sound signals that propagate through the air are scattered by turbulence, which causes random fluctuations in the measured data [1]–[3]. In past work [4], we have studied passive time-delay estimation with widely-separated aeroacoustic sensors. We found that accurate time-delay estimates are difficult to obtain for many ground vehicles because their engines emit a harmonic spectrum with small time-bandwidth product, and also because the scattering causes a loss in signal coherence.

In this paper, we study Doppler estimation for moving acoustic sources. Doppler estimation is important because it provides information about the path of a moving source, and it may be combined with bearing estimates for improved localization accuracy. The narrowband, harmonic spectrum of the source is advantageous for Doppler estimation, and the differential Doppler between two sensors can be estimated *noncoherently*. We provide a statistical performance analysis of differential Doppler estimation using the scattering propagation model summarized in [3]. We provide Cramér-Rao bounds (CRBs) on the accuracy of differential Doppler estimation as a function of signal-to-noise ratio (SNR), meteorological conditions, frequency of the source, and the range of the source. We compare the performance of frequency estimation algorithms with the CRB, and we present results from processing measured aeroacoustic data.

2. DATA MODEL

In this section, we present a model for the signals received by a network of aeroacoustic sensors. We focus on acoustic sources with harmonic spectra, which are generated by rotating machinery in engines, tire and/or exhaust noise, vibrating surfaces, and other effects. Internal combustion engines typically exhibit a strong harmonic acoustic signature tied to the cylinder firing rate.

We begin by considering a moving source that emits a single tone, and we present a model for the scattering caused by atmospheric turbulence. The model is extended to moving sources that emit a sum of harmonics by assuming that the scattering in each harmonic is independent. The model is formulated for a single sensor, but it may be extended to multiple sensors by modeling the scattering and noise as independent at distinct sensors. The scattering is independent if the distance between the sensors is larger than a few 10's of m [3]. The scattering model was developed by Wilson, Collier, and others [1]–[2]. The book chapter [3] presents the scattering model for a nonmoving source, so the reader may refer to [3] for more details and additional references.

Four phenomena are primarily responsible for modifying a sinusoidal signal emitted by a nonmoving source to produce the signal observed at the sensor:

1. Transmission loss caused by spreading of the wavefronts, refraction by wind and temperature gradients, ground interactions, and molecular absorption.

2. The propagation delay from the source to the sensors.

3. Additive noise at the sensors caused by thermal noise, wind noise, and directional interference.

4. Random fluctuations in the amplitude and phase of the signals caused by scattering from random inhomogeneities in the atmosphere such as turbulence.

The propagation delay is developed using a path for the source that is a straight line with constant velocity over an observation interval of length T sec, $t \in [t_o, t_o + T]$. If the radial velocity of the source is denoted by $v_r(t_o)$, then the propagation time is well-approximated by [5]

$$\tau(t) \approx \tau(t_o) + \frac{1}{c}v_r(t_o)(t - t_o), \qquad (1)$$

where c is the speed of sound.

The scattering of the signal by turbulence is particularly significant. The turbulence consists of random atmospheric motions occurring on time scales from seconds to several minutes. Scattering from these motions causes random fluctuations in the complex signals at the sensor. The random fluctuations caused by scattering are modeled as a complex, circular, Gaussian random process with zero mean. The Gaussian model for the scattering is somewhat idealized, but it has been shown experimentally to be accurate in many cases of interest [6, 7, 8].
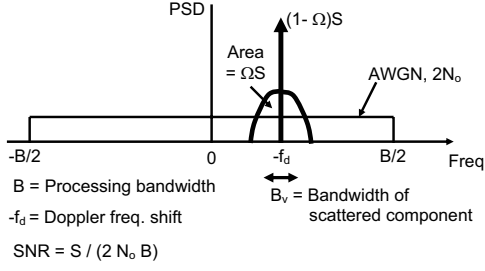
Fig. 1. PSD $G_{\tilde{z}}(f)$ for the sensor signal model in (2) for processing bandwidth B Hz.

The scattering spreads a portion of the energy from the pure tone emitted by the source into a zero-mean random process, which we denote by $\tilde{v}(t)$. The *saturation* parameter [2], denoted by $\Omega \in [0,1]$, defines the fraction of average signal power that is scattered from the mean into the random component. The model for the complex envelope of the sensor signal is

$$\tilde{z}(t) = \tilde{s}[t - \tau(t)] + \tilde{w}(t)$$
$$= \sqrt{(1-\Omega)S} \exp[j\theta] \exp[-j2\pi f_d(t - t_o)]$$
$$+ \sqrt{\Omega S}\,\tilde{v}(t) \exp[j\theta] \exp[-j2\pi f_d(t - t_o)]$$
$$+ \tilde{w}(t), \tag{2}$$

where the complex envelope is computed with respect to the source frequency, f_o. The noise, $\tilde{w}(t)$, is AWGN (complex, circular, Gaussian random process with zero mean) with power spectral density (PSD) $G_{\tilde{w}}(f) = 2\mathcal{N}_o$. The average signal energy, $E\{|\tilde{s}(t)|^2\} = S$, is determined by the source strength and transmission loss. The phase θ in (2) is determined by the source phase and the propagation time $\tau(t_o)$ in (1). The frequency, $-f_d$, is the shift due to Doppler, and it depends on the radial velocity of the source and the frequency of the source,

$$f_d = \frac{v_r(t_o)}{c} f_o = \text{Doppler frequency shift.} \tag{3}$$

The scattering may be *weak* ($\Omega \approx 0$) or *strong* ($\Omega \approx 1$), which are analogous to Rician and Rayleigh fading in the radio propagation literature. The scattered process $\tilde{v}(t)$ has PSD $G_{\tilde{v}}(f)$, which we model as a symmetric function centered at 0 Hz with bandwidth B_v Hz. This implies that the autocorrelation function, $r_{\tilde{v}}(\xi)$, is real-valued with coherence time on the order of $1/B_v$ sec. The scattered process is normalized to unit average power, $r_{\tilde{v}}(0) = 1$.

The PSD $G_{\tilde{z}}(f)$ corresponding to the model in (2) is illustrated in Figure 1, and the corresponding formula is

$$G_{\tilde{z}}(f) = (1-\Omega)S\,\delta(f + f_d) + (\Omega S)\,G_{\tilde{v}}(f + f_d) + G_{\tilde{w}}(f).$$

The observations are band-pass filtered with bandwidth B Hz, so the AWGN PSD is $G_{\tilde{w}}(f) = 2\mathcal{N}_o \, \text{rect}(f/B)$, where B must be larger than the maximum Doppler frequency shift for the source of interest. Our objective in this paper is to study algorithms and performance bounds for estimating f_d in Figure 1 as a function of the saturation Ω, the processing bandwidth B Hz, the observation time T, the average SNR $= S/(2\mathcal{N}_o B)$, and the scattered bandwidth B_v.

The sensor signals in (2) with PSD in Figure 1 may be sampled at the rate $F_s = B$ samples per second, so the spacing between samples is $T_s = 1/B$. In the observation time of T sec,

$N = \lfloor BT \rfloor$ samples are obtained, which are collected in the vector $\tilde{\mathbf{z}} = \begin{bmatrix} \tilde{z}(0) & \ldots & \tilde{z}((N-1)T_s) \end{bmatrix}^T$. This vector has a complex Gaussian distribution with mean and covariance matrix

$$\tilde{\mathbf{z}} \sim \text{CN}\left(e^{j\theta}\sqrt{(1-\Omega)S}\,\mathbf{a},\right.$$
$$\left. (\Omega S)\,\mathbf{R}_{\tilde{v}} \circ \left(\mathbf{a}\mathbf{a}^H\right) + (2\mathcal{N}_o B)\mathbf{I}\right), \tag{4}$$

where

$$\mathbf{a}^T = [1, \exp\left(-j2\pi f_d/B\right), \ldots, \exp\left(-j2\pi(N-1)f_d/B\right)],$$

$\mathbf{R}_{\tilde{v}}$ is the covariance matrix of the samples of the scattered process with elements $[\mathbf{R}_{\tilde{v}}]_{mn} = r_{\tilde{v}}[(m-n)/B]$, $\circ$ denotes element-wise product, $(\cdot)^H$ denotes Hermitian transpose, and $\mathbf{I}$ is the identity matrix.

The scattering causes fluctuations in the signal energy at the sensor. A plot of the probability density function (pdf) of $10 \log_{10} |\tilde{z}(t)|^2$ is presented in [3], showing that small deviations in the saturation from $\Omega = 0$ cause energy fluctuations of several dB. For $\Omega > 0.5$, energy deviations of 10 to 15 dB are not uncommon.

The value of the saturation Ω at a sensor depends on the source distance (d), the source frequency (f_o), and the meteorological conditions. The saturation Ω depends on the source range, d, according to [3]

$$\Omega = 1 - \exp\left(-2\,\mu\,d\right), \tag{5}$$

where μ is called the extinction coefficient for the first moment. An approximate expression for μ as a function of frequency and meteorological condition is [3]

$$\mu \approx \begin{cases} 4.03 \times 10^{-7} f_o^2, & \text{mostly sunny} \\ 1.42 \times 10^{-7} f_o^2, & \text{mostly cloudy} \end{cases}, \tag{6}$$

for $f_o \in [30, 200]$ Hz. A contour plot of (5) and (6) for mostly sunny conditions is contained in [3]. The plot shows that Ω values over the entire range from 0 to 1 may be encountered in aeroacoustics for frequencies in the range from 30 to 200 Hz and ranges from 5 to 200 m. The saturation varies significantly with frequency for ranges > 100 m.

3. CRAMÉR-RAO BOUNDS

The CRB provides a lower bound on the variance of any unbiased estimate $\hat{f}_d$, so $E\{|\hat{f}_d - f_d|^2\} \geq \text{CRB}(\hat{f}_d)$. The general form of the CRB for a complex Gaussian model such as (4) is well-known, e.g., [9]. Schultheiss and Weinstein [10] derived closed-form expressions for the CRBs in the particular cases when $\Omega = 0$ (no scattering) and $\Omega = 1$ (full scattering):

$$\Omega = 0 : \text{CRB}(\hat{f}_d) = \frac{3}{2\pi^2 T^3} \frac{\mathcal{N}_o}{S} \tag{7}$$

$$\Omega = 1 : \text{CRB}(\hat{f}_d) \approx \frac{B_v/T}{\int_0^\infty \left(\frac{d}{dx}\log G_1(x)\right)^2 dx}. \tag{8}$$

For $\Omega = 1$, the approximation is accurate for high SNR $= S/(2\mathcal{N}_o B)$ and large $B_v T =$ time-bandwidth product of the scattered process. The function $G_1(x)$ in (8) is a normalized form of the scattered PSD with unit bandwidth, so that $G_{\tilde{v}}(f) = (1/B_v)\,G_1(f/B_v)$.

Next we evaluate the CRBs on frequency estimation for Ω in the interval $[0, 1]$. We use the following form for the scattered PSD,

$$G_{\tilde{v}}(f) = \frac{\beta}{B_v}\text{tri}\left(\frac{f}{B_v}\right) + \frac{1-\beta}{B}\text{rect}\left(\frac{f}{B}\right), \qquad (9)$$

where $\text{tri}(x) = 1 - |x|$ for $|x| \le 1$ and 0 otherwise, $\text{rect}(x) = 1$ for $|x| \le 0.5$ and 0 otherwise, and $\beta = 0.95$ determines the fraction of energy in the "peaked" triangular function that has bandwidth B_v. The broader, rectangular component is added to (9) in order to prevent the PSD from reaching the value of 0, which leads to optimistic CRBs. The autocorrelation function of the scattered process is $r_{\tilde{v}}(\xi) = \beta\,\text{sinc}^2(B_v\xi) + (1 - \beta)\,\text{sinc}(B\xi)$.

The CRBs for several cases are shown in Figures 2(a) and 2(b). The exact CRB based on the model (4) is indicated by the solid line for $\Omega \in [0, 1]$, while the Schultheiss & Weinstein (S-W) CRBs for $\Omega = 0$ and $\Omega = 1$ in (7) and (8) are indicated by $*$. Figure 2(a) shows the CRB variation with saturation Ω and scattered signal bandwidth B_v. (The values of all parameters are specified in the caption to Figure 2.) The CRB with no scattering ($\Omega = 0$) is independent of B_v and agrees with the S-W formula in (7). With full scattering ($\Omega = 1$), the CRB agrees with the S-W approximation in (8) when $B_vT > 1$. Note that the CRB increases rapidly for small values of $\Omega > 0$, and then the variation is fairly flat with Ω. Figure 2(b) shows the CRB variation with saturation Ω and observation time T. Again we see the agreement with the S-W formula in (7) for all values of T and (8) for $B_vT > 1$, and the rapid increase in the CRB for small values of $\Omega > 0$. For parameter values that are commonly encountered in aeroacoustics, e.g., $B_v = 0.1$ Hz, $T = 1$ sec, and $\underline{\text{SNR}} = 30$ dB, Figure 2 indicates that scattering increases the $\sqrt{\text{CRB}}$ by a factor of 10.

We have also investigated the CRB variation with average SNR. The CRB is inversely proportional to SNR with no scattering ($\Omega = 0$), as in (7), and is fairly insensitive to SNR for $\Omega > 0$ (note (8) is independent of SNR for $\Omega = 1$).

Estimators for f_d based on the model (4) are considered next. We do not consider the general case in which the saturation $\Omega \in [0, 1]$ is unknown. Instead, we consider the maximum-likelihood (ML) estimator for the case of no scattering ($\Omega = 0$) and an estimator that was proposed by Besson and Stoica [11] for the case of full scattering ($\Omega = 1$). The periodogram (P-GRAM) is the ML estimator with no scattering, and is given by

$\widehat{f}_d = \underset{f_d}{\text{argmax}} \left| \sum_{n=0}^{N-1} \tilde{z}(nT_s)\,\exp(j2\pi f_d\,nTs) \right|^2$. For the case

of full scattering ($\Omega = 1$), the signal component in (4) is a random process with unknown covariance matrix $\mathbf{R}_{\tilde{v}}$. For the case in which $\mathbf{R}_{\tilde{v}}$ is real-valued, Toeplitz, and unknown, Besson and Stoica [11] proposed the following estimator:

$\widehat{f}_d = \underset{f_d}{\text{argmax}} \ \text{Re}\left\{ \sum_{m=1}^{N-1} \widehat{r}_{\tilde{z}}[m]^2\,\exp(j4\pi f_d\,mTs) \right\}$, where

$\widehat{r}_{\tilde{z}}[m]$ is a consistent estimate of the mth lag of the sensor signal autocorrelation. We label this estimator C^2-GRAM because it is similar to the correlogram.

Figure 2(c) contains simulated mean-squared error (MSE) results for both estimators for the range of saturation values $\Omega \in [0, 1]$ and the parameter values listed in the caption. The P-GRAM and C^2-GRAM estimators perform similarly for the conditions in these simulations. The MSEs of both estimators are close to the CRB for $\Omega < 0.1$, then the MSE diverges from the CRB for larger values of Ω. We note that the CRB for $\Omega > 0$ is optimistic since it
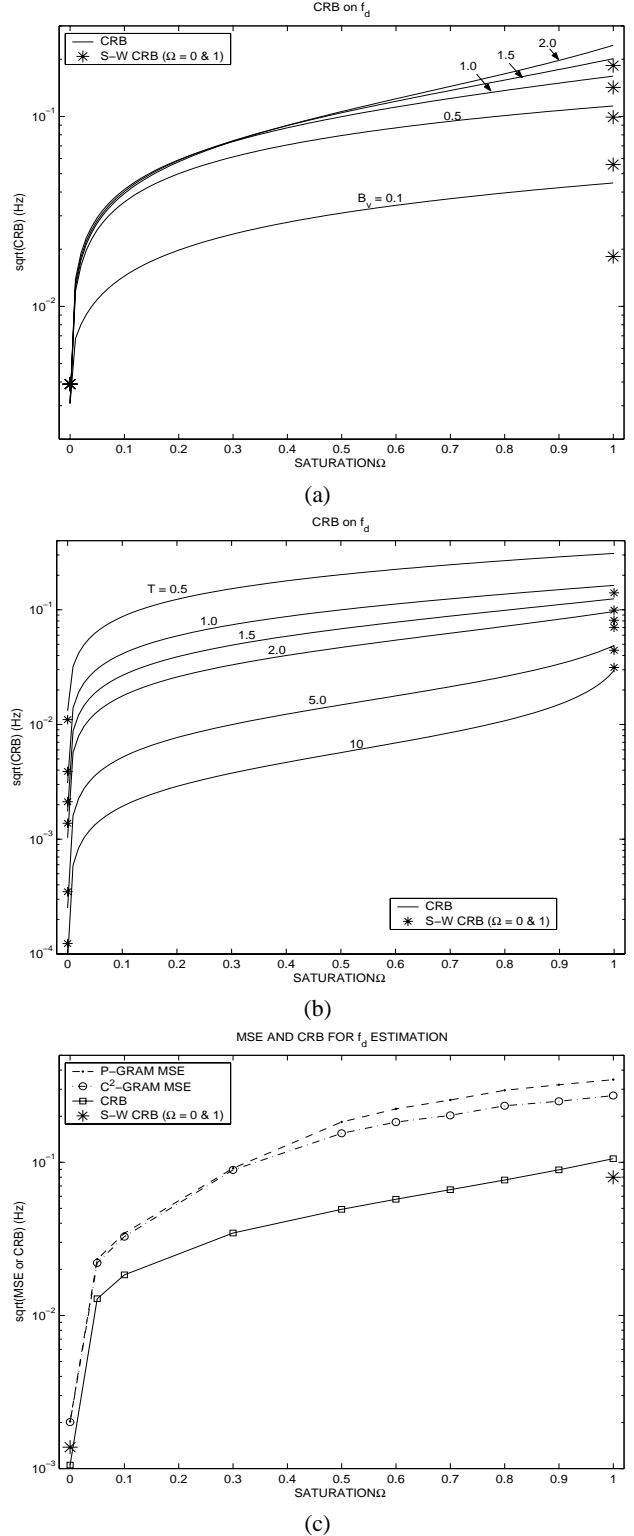

(a)

(b)

(c)

Fig. 2. CRBs for estimation of f_d with $f_d = -0.2$ Hz, SNR $= 28.5$ dB, $B = 7$ Hz, and (a) $T = 1$ sec, and various B_v; (b) $B_v = 1$ Hz, and various T. (c) Comparison of frequency estimation mean-squared error (MSE) with the CRB for $B = 5$ Hz, $T = 2$ sec, average SNR $= 30$ dB, $B_v = 1$ Hz, and $f_d = 0.31$ Hz.

Freq. (Hz)	Range (m)						
	5	10	20	40	80	160	320
45	.004	.008	.016	.032	.063	.122	.230
90	.016	.032	.063	.122	.230	.409	.648
135	.036	.071	.137	.255	.444	.691	.905
180	.063	.122	.230	.407	.648	.876	.985

(a)

Freq. (Hz)	Range (m)						
	5	10	20	40	80	160	320
45	.004	.006	.008	.013	.019	.031	.053
90	.007	.010	.015	.023	.034	.054	.096
135	.011	.015	.022	.032	.049	.078	.145
180	.014	.020	.028	.041	.061	.097	.171

(b)

Table 1. (a) Saturation Ω for harmonic frequencies at various ranges under mostly sunny conditions using (5),(6). (b) $\sqrt{\text{CRB}}$ on Doppler for harmonics at various ranges.

Fig. 3. Differential Doppler estimates from measured data.

is derived for the case in which Ω, SNR, and $\mathbf{R}_{\tilde{v}}$ are known. Additional simulations indicate that for $\Omega > 0.5$, the MSEs are fairly insensitive to the SNR and B_v values.

4. EXAMPLES

We consider Doppler estimation for a harmonic source at various ranges using the model for saturation in (5) and (6). Let the fundamental frequency of the source be 15 Hz, and suppose that harmonics 3, 6, 9, and 12 (at 45, 90, 135, and 180 Hz) are used for Doppler estimation. Then the saturation Ω varies with frequency and range as in Table 1(a).

We consider a processing bandwidth $B = 10$ Hz, observation time $T = 2$ sec, and scattering bandwidth $B_v = 0.5$ Hz. The SNR is varied in proportion to $1/\text{range}^2$, resulting in SNR variations from 33 dB at range 5 m to -3 dB at range 320 m. Table 1(b) contains the $\sqrt{\text{CRB}}$ on Doppler frequency estimation for each frequency and range. The $\sqrt{\text{CRB}}$ on Doppler estimation is smaller at the 45 Hz harmonic than the 180 Hz harmonic by about a factor of 3 at each range. The $\sqrt{\text{CRB}}$ gets larger by about an order of magnitude between source ranges 10 m and 320 m.

Figure 3 shows the estimated differential Doppler shift between two sensors based on measured aeroacoustic data. A tracked vehicle traveled between the sensors at a range of about 100 m from each sensor, and a frequency component near 38 Hz was estimated during a 10 sec time interval. Note from the MEAN ESTIMATE line that smoothing the Doppler estimates over time provides an error from GPS ground truth that is comparable to $\sqrt{\text{CRB}} \approx 0.1$ Hz, where the CRB is computed for conditions that approximate those in the experiment.

5. REFERENCES

[1] S.L Collier and D.K. Wilson, "Performance bounds for passive arrays operating in a turbulent medium: Plane-wave analysis," *J. Acoust. Soc. Am.*, Vol. 113, No. 5, pp. 2704–2718, May 2003.

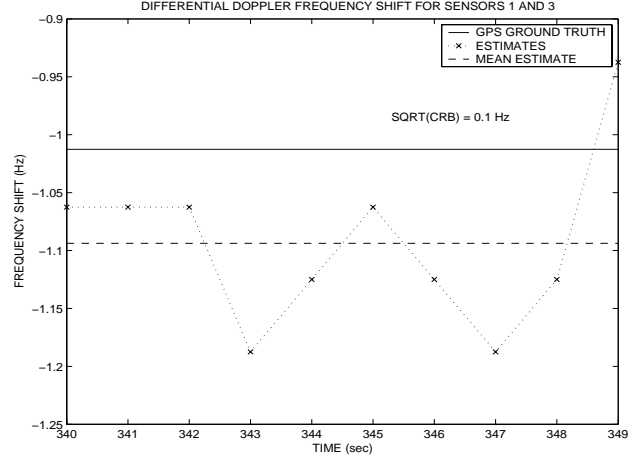[2] D. E. Norris, D. K. Wilson, and D. W. Thomson, "Atmospheric scattering for varying degrees of saturation and turbulent intermittency," *J. Acoust. Soc. Am.*, vol. 109, pp. 1871–1880, 2001.

[3] R.J. Kozick, B.M. Sadler, and D.K. Wilson, "Signal Processing and Propagation for Aeroacoustic Sensor Networking," to appear in *Frontiers in Distributed Sensor Networks*, S.S. Iyengar and R.R. Brooks (Eds.), CRC Press, 2004.

[4] R.J. Kozick and B.M. Sadler, "Source localization with distributed sensor arrays and partial spatial coherence," to appear in *IEEE Trans. on Sig. Proc.*, March 2004.

[5] R.J. Kozick and B.M. Sadler, "Tracking Moving Acoustic Sources with a Network of Sensors," Army Research Laboratory Technical Report ARL-TR-2750, October 2002.

[6] G. A. Daigle, J. E. Piercy, and T. F. W. Embleton, "Line-of-sight propagation through atmospheric turbulence near the ground," *J. Acoust. Soc. Am.*, vol. 74, pp. 1505–1513, 1983.

[7] H. E. Bass, L. N. Bolen, R. Raspet, W. McBride, and J. Noble, "Acoustic propagation through a turbulent atmosphere: experimental characterization," *J. Acoust. Soc. Am.*, vol. 90, pp. 3307–3313, 1991.

[8] D.E. Norris, D.K. Wilson, D.W. Thomson, "Correlations between acoustic travel-time fluctuations and turbulence in the atmospheric surface layer," *Acta Acustica*, vol. 87, pp. 677–684, 2001.

[9] S.M. Kay, *Fundamentals of Statistical Signal Processing: Estimation Theory*, Prentice-Hall, 1993.

[10] P.M. Schultheiss and E. Weinstein, "Estimation of differential Doppler shifts," *J. Acoust. Soc. Am.*, vol. 66, no. 5, pp. 1412-1419, Nov. 1979.

[11] O. Besson and P. Stoica, "On frequency offset estimation for flat-fading channels," *IEEE Communications Letters*, vol. 5, no. 10, pp. 402–404, Oct. 2001.